Original Research Article

OPTIMIZING DISTRIBUTION TRANSFORMER DESIGN FOR HARMONIC RESILIENCE: A TAGUCHI-FEM APPROACH

Abstract

The Nigeria's low-voltage distribution transformers suffer from significant harmonic issues leading to catastrophic failures. Existing strategies to address harmonics have overlooked transformer inherent parameter design optimizations. This study presents the optimization of a 30 kVA transformer, focusing on enhancing efficiency and minimizing harmonic susceptibility for low-voltage distribution systems in Nigeria. Utilizing a combined Taguchi-FEM approach, key design parameters such as core area (0.773 m^2), material (Amorphous Steel), core design (Six-Stepped Core), and flux density (1.354T) were optimized, resulting in a 27% reduction in energy losses. Finite Element Analysis (FEA) revealed that the optimized transformer exhibited a core saturation of 19.2%, significantly lower than the baseline's 42%, and demonstrated reduced energy density near the core-winding interface. Experimental validation through Open Circuit (OC) and Short Circuit (SC) tests confirmed a notable improvement in efficiency, with the optimized transformer achieving 97.15% efficiency at full load, compared to 95.5% for the baseline transformer. Core losses were reduced to 85W, and copper losses decreased to 800W. The findings align with international standards (IEC 60076-8). Optimizing core materials and stepped core design with advanced modeling can enhance reliability and reduce harmonic impacts. Therefore, integrated optimization approaches, incorporating Taguchi-FEM and experimental techniques, can effectively enhance transformer performance, paving the way for broader applications in the field.

Keywords: Transformer Optimization; Finite Element Analysis; Harmonic Susceptibility; Taguchi Method; Energy Density; Low-Voltage Distribution Systems

Introduction

Distribution transformers are evolving to support energy efficiency, advanced monitoring, and environmental goals essential for modern grids and renewable energy integration (Worku, 2022). Yet, these systems face challenges from dynamic load demands, environmental pressures, and complex power distribution, all of which strain transformer reliability and performance (Huang & Hsieh, 2013). One primary concern is harmonics, which escalate transformer losses and reduce efficiency. Harmonic distortions pose unique obstacles, underscoring the need for transformer design refinement focused on harmonic resilience. Traditional transformer designs often overlook harmonic-specific optimizations, which can enhance transformer durability and resilience under nonlinear conditions (Kraszewski et al., 2022). Flexible, optimized transformer designs are therefore essential to improving power system efficiency, minimizing downtime, and extending transformer lifespan. Optimizing key parameters like core material and stepped core design, combined with advanced modeling techniques, can mitigate harmonic effects while strengthening system reliability (Baldwin et al., 2013).

The Taguchi is one optimization method which uses orthogonal arrays to isolate optimal settings, enhances design reliability by focusing on Signal-to-Noise (S/N) ratios, ensuring consistency across variable conditions (Ntemi et al., 2022). Finite Element Method (FEM) simulations provide detailed insights into electromagnetic and thermal behavior, using tools like ANSYS Maxwell to refine magnetic performance and evaluate stress distribution with high precision (SIMTEQ Engineering, 2024). According to Barua et al. (2018), the Taguchi-FEM approach streamlines design experimentation, enabling cost-effective yet high-performance optimizations. This method ensures reliable, resilient transformer designs that meet the needs of sustainable, stable power grids, minimizing harmonic impacts and supporting transformer longevity. The Taguchi method, optimizes quality and performance in various fields by minimizing variability and costs while enhancing product quality through Design of Experiments (DOE), S/N ratios, and parameter optimization (Vuchkov & Boyadjieva, 2001). DOE allows engineers to efficiently adjust input factors to observe their impacts on performance (Box, Hunter & Hunter, 2005). The S/N ratio maximizes signal strength relative to noise, stabilizing outputs (Hamzaçebi, 2020), while parameter optimization utilizes orthogonal arrays to identify

optimal settings (Oliveira, 2022). Applications of the Taguchi method encompass manufacturing and product design, focusing on process optimization to reduce variability and enhance customer satisfaction (Barua et al., 2018). Its systematic approach effectively develops high-quality products (Karna & Sahai, 2012).

FEA with ANSYS Maxwell is crucial for optimizing engineering systems, particularly for electromagnetic and structural analyses. ANSYS Maxwell employs the FEM to solve Maxwell's equations, providing insights into electromagnetic field simulations for components like transformers and motors, optimizing efficiency and robustness. It supports static, steady-state, and transient analyses, utilizing adaptive mesh refinement for precision. The combined Taguchi-FEM approach significantly enhances distribution transformer design optimization (Ogedengbe & Mekid, 2011). The Taguchi DOE identifies critical design parameters, while FEM offers precise analyses of electromagnetic fields and thermal behavior. This hybrid method reduces experiment counts by systematically varying parameters, improving robustness and energy efficiency, ultimately leading to reliable transformers capable of withstanding operational challenges.

Geetha et al. (2024) optimized power transformer parameters using Taguchi's L9 array and ANSYS Maxwell, focusing on core loss reduction in an 8MVA, 33/11KV transformer. They achieved a 4.568 kW loss at optimal core area, voltage, and material settings. Pramono et al. (2023) used particle swarm optimization to reduce noise, weight, and losses in power transformers, validated via COMSOL. Achieving a 0.86dB-SNR noise reduction, core weight decreased by 2.12%, and winding weight by 47.46%. Olivares-Galvan et al. (2023) minimized the total owning cost of a 750 kVA transformer using genetic, swarm, and differential evolution algorithms, reducing TOC by 6%. Arkadan and Gutierrez-McCoy (2023) developed an optimized design approach for power transformers, combining finite-element state-space (FE-SS) models, artificial neural networks (ANNs), and particle swarm optimization (PSO). A 42 MVA transformer case study validated the model, showing alignment with test data. Taguchi orthogonal arrays (OA) reduced computational costs, enhancing efficiency. Their approach effectively demonstrated improved transformer performance through advanced modeling and optimization. Rasmann et al. (2023) automated the planar transformer design process for high-frequency applications. Using Design Automation (DA) with 2D FEM simulations and an Evolutionary Algorithm (EA), they efficiently optimized parasitic elements, streamlining traditionally manual processes. Hacan et al. (2022) optimized a 1kVA transformer's volume and loss with a differential evolution algorithm in ANSYS Maxwell. They achieved 91.50% efficiency at 75% load. Outzguinrimt et al. (2020) optimized transformer mass and volume in MATLAB-Simulink, reducing core mass from 29 kg to 16.59 kg. Xinsheng et al. (2020) used a multi-objective optimization approach, reducing copper loss by 4.5% and manufacturing cost by 3.89% using a GDE3 algorithm and FEM. Di-Noia et al. (2017) minimized the total owning cost of transformers with amorphous cores, achieving significant loss reductions in ANSYS Maxwell. Sarac (2017) simulated core losses and magnetic flux distribution in transformers using FEM, noting specific flux densities at various core areas. Tsili et al. (2012) combined the Taguchi method with FEM for multi-winding transformer optimization, minimizing short-circuit impedance deviations. Though most of the studies attempt to optimize transformer design, their focus was either on cost, material, mass, volume, impedance, and noise reduction. However, neglecting harmonics mitigation especially in low voltage transformers.

In the case of Nigeria's power grid, low-voltage networks face severe harmonic issues, often leading to transformer failures due to factors like frequent switching operations, outdated equipment and insufficient grounding. Existing system-level strategies address harmonics, but do not fully exploit potential transformer design optimizations (Abdulhamid, 2020; Koledowo et al., 2020). Therefore, this study applies a hybrid Taguchi-FEM approach to design distribution transformers with improved harmonic resilience. Through optimization of core area, flux density, and other critical parameters, the research aims to enhance transformer performance, improve efficiency, stability, and economic viability in Nigeria's distribution sector.

Methods

The study employed a combined Taguchi and FEA approach to optimize transformer design for low-voltage distribution systems, specifically targeting harmonic impact resilience and loss minimization. The baseline transformer specifications (Table 1) were used characterize the optimized transformer core parameters including core area, core material and flux density. These were then optimized using the Taguchi method for robust SNR analysis, while FEM was employed to validate the Taguchi optimal settings; through modeling and simulation with ANSYS Maxwell.

Table 1: Parameters of the baseline transformer

Parameter	Specification
Rated Power	30 kVA
Primary Voltage	11 kV
Secondary Voltage	0.415 kV
Frequency	50 Hz
Vector Group	Dyn11
No-load Loss	340 W
Load Loss (75°C)	1070 W
Load Loss (120°C)	1230 W
No-load Current	2.4%
Maximum Current Density	2.5 A/m²
Short Circuit Impedance	6%
Noise Level	48 dB
Maximum Flux Density	1.7 T
Maximum Efficiency	95.5%
Total Weight	490 kg
Dimension (L/W/H)	1180/780/810 mm
Cooling Mode	AN
Winding Material (HV)	Copper/Copper
Phase	1 phase/3 phases

The Taguchi Design of Experiments

The Taguchi Robust Approach for Multi-Objective Design Optimization was applied systematically to achieve targeted objectives. Initially, multiple objectives such as minimizing losses, maximizing efficiency, and mitigating harmonic effects were clearly defined. Four control variables were then selected: core area, core material, core design type, and flux density. These factors were mapped based on laboratory investigations. An L9 orthogonal array (presented in Table 2) was chosen for the DOE, allowing a structured approach with a three-level experimental run for each selected factor. This setup facilitated a systematic variation of design parameters using the Taguchi method. Data collection followed, as each experiment from the DOE plan was conducted, gathering results for each unique configuration of design parameters.

Table 2: The L9 orthogonal array for four factors, three levels

Experiment Run	Factor A	Factor B	Factor C	Factor D
1	1	1	1	2
2	1	2	2	3
3	1	3	3	1
4	2	1	2	3
5	2	2	3	1
6	2	3	1	2
7	3	1	3	1
8	3	2	1	2
9	3	3	2	3

This analysis identified optimal design parameters, effectively addressing harmonic mitigation while achieving the other design objectives. The workflow for this Taguchi robust approach is illustrated in Figure 1.

Selected Factors (Control Variables)

i. **Core Area**: The core area affects the magnetic flux and the overall size of the transformer. Larger core areas can handle higher flux densities but may increase material costs.

ii. **Core Material**: The material of the core determines the core losses and magnetic properties. M3 grade silicon steel is commonly used for its low core losses and high permeability. M6 is a bit more standard, and amorphous steel offers the lowest losses but can be more expensive.

iii. **Core Design Type**: The core design affects the efficiency and performance of the transformer. A square core is simple and cost-effective, while stepped core designs improve magnetic flux distribution and reduce losses.

iv. **Flux Density**: The flux density impacts the transformer's performance and core losses. Operating at higher flux densities can reduce the core size but increases core losses. Lower flux densities reduce core losses but require larger cores.

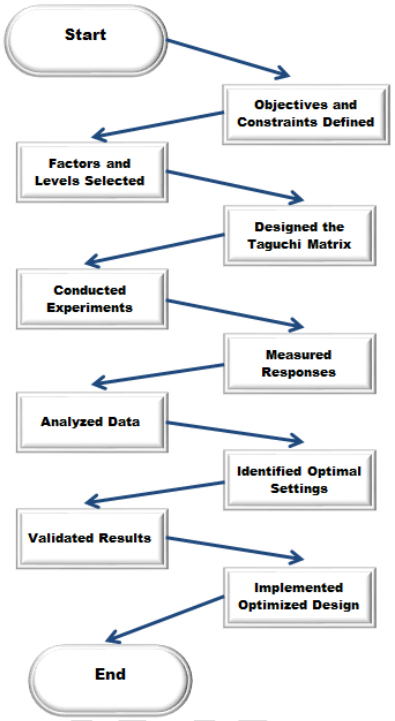

Figure 1: Taguchi Robust Workflow Diagram

Factor Levels and Rationale

For the Taguchi DOE, four factor levels were selected to optimize transformer performance, focusing on minimizing losses, maximizing efficiency, and mitigating harmonic effects.

Core Area: Adjusted by 6% to evaluate core area sensitivity within typical manufacturing tolerances.

Core Materials: M5, M6, and Amorphous, chosen for their documented magnetic properties and industry use in high-efficiency applications.

Core Design Types: Square, three-stepped, and six-stepped cores were chosen to test flux distribution and manufacturability.

Flux Density: Adjusted by 6% to reflect manufacturing variations and to study effects on core saturation and magnetic losses.

Orthogonal Array Selection

An $L_9(3^4)$ orthogonal array was used, accommodating four factors at three levels each. This ensured an efficient DOE setup, providing robust, balanced results through orthogonality principles for reliable performance analysis. Thus for a start; basic cyclic patterns were employed to fill in the factor level combinations in the initial columns C_1, C_2 and C_3. Therefore:

$$\text{Column } C_1 = \begin{bmatrix} 1 \\ 1 \\ 1 \\ 2 \\ 2 \\ 2 \\ 3 \\ 3 \\ 3 \end{bmatrix} \quad (1)$$

Then Column C_2 was generated by cycling through the levels at a different rate from C_1. Thus:

$$\text{Column } C_2 = \begin{bmatrix} 1 \\ 2 \\ 3 \\ 1 \\ 2 \\ 3 \\ 1 \\ 2 \\ 3 \end{bmatrix} \quad (2)$$

And for Column C_3, the cyclic pattern was initialized and continued in such a way that it complemented Columns C_1 and C_2, ensuring that no level combination was repeated more than once in any row combination. Thus:

$$\text{Column } C_3 = \begin{bmatrix} 1 \\ 2 \\ 3 \\ 2 \\ 3 \\ 1 \\ 3 \\ 1 \\ 2 \end{bmatrix} \quad (3)$$

And finally Column C_4 was generated by adding the corresponding elements of Columns C_1 and C_2 using modular arithmetic (mod_3) to ensure that the values are within the required range. So that:

$$C_4 = (C_1[i]) + C_2[i] \text{ (mod 3)} \quad (4)$$

Implying that:

$$\text{Column } C_4 = \text{Column} \left(C_1 = \begin{bmatrix} 1 \\ 1 \\ 1 \\ 2 \\ 2 \\ 2 \\ 3 \\ 3 \\ 3 \end{bmatrix} \right) + \text{Column} \left(C_2 = \begin{bmatrix} 1 \\ 2 \\ 3 \\ 1 \\ 2 \\ 3 \\ 1 \\ 2 \\ 3 \end{bmatrix} \right) \quad (5)$$

So that:
For row 1: $1 + 1 = 2 \text{ (mod 3)} = 2$
For row 2: $1 + 2 = 3 \text{ (mod 3)} = 3$
For row 3: $1 + 3 = 4 \text{ (mod 3)} = 1$ (since 4 mod $3 = 1$)
For row 4: $2 + 1 = 3 \text{ (mod 3)} = 3$
For row 5: $2 + 2 = 4 \text{ (mod 3)} = 1$
For row 6: $2 + 3 = 5 \text{ (mod 3)} = 2$
For row 7: $3 + 1 = 4 \text{ (mod 3)} = 1$

For row 8: $3 + 2 = 5 \pmod 3 = 2$
For row 9: $3 + 3 = 6 \pmod 3 = 3$
And then:

$$\text{Column } C_4 = \begin{bmatrix} 2 \\ 3 \\ 1 \\ 3 \\ 1 \\ 2 \\ 1 \\ 2 \\ 3 \end{bmatrix} \quad (6)$$

The columns C_1, C_2, C_3 and C_4 were then arranged into a matrix table to form the L9 orthogonal array with the selected factors and level (experimental runs/trials) assigned to the respective columns and rows accordingly. Table 3 illustrates the mapping of the selected factors to align them with the general A, B, C, D IDs, along with their corresponding levels. Factor A, representing Core Area, was categorized into three levels: A1 for Small, A2 for Medium, and A3 for Large core areas. Factor B, designated as Core Material, was assigned levels B1 for Material 1 (M5), B2 for Material 2 (M6), and B3 for Material 3 (Amorphous Steel). Factor C, concerning the Stepped Core Design, included levels C1 for Core Design 1, C2 for Core Design 2, and C3 for Core Design 3. Lastly, Factor D, representing Flux Density, was mapped to D1 for Low, D2 for Medium, and D3 for High flux densities. This systematic alignment ensured that the L9 Orthogonal Array effectively captures the influence of these key factors on the transformer's performance, facilitating a thorough and balanced analysis. Table 4 reflects the mapping of the selected factors (Core Area, Core Material, Stepped Core Design, and Flux Density) to the L9 Orthogonal Array.

Table 3: Mapping of selected factors with general IDs and levels

Factor	**ID**	**Levels**
Core Area	A	A1: Small, A2: Medium, A3: Large
Core Material	B	B1: (Material 1), B2: (Material 2), B3: (Material 3)
Stepped Core Design	C	C1: (Core Design 1), C2: (Core Design 2), C3: (Core Design 3)
Flux Density	D	D1: Low, D2: Medium, D3: High

Table 4: Mapping to L9 orthogonal array

Experiment Run	**Factor A: Core Area**	**Factor B: Core Material**	**Factor C: Stepped Core Design**	**Factor D: Flux Density**
1	A1 (Small)	B1 (Material 1)	C1 (Core Design 1)	D2 (Medium)
2	A1 (Small)	B2 (Material 2)	C2 (Core Design 2)	D3 (High)
3	A1 (Small)	B3 (Material 3)	C3 (Core Design 3)	D1 (Low)
4	A2 (Medium)	B1 (Material 1)	C2 (Core Design 2)	D3 (High)
5	A2 (Medium)	B2 (Material 2)	C3 (Core Design 3)	D1 (Low)
6	A2 (Medium)	B3 (Material 3)	C1 (Core Design 1)	D2 (Medium)
7	A3 (Large)	B1 (Material 1)	C3 (Core Design 3)	D1 (Low)
8	A3 (Large)	B2 (Material 2)	C1 (Core Design 1)	D2 (Medium)
9	A3 (Large)	B3 (Material 3)	C2 (Core Design 2)	D3 (High)

The objective function is the losses minimization; and thus; our targeted quality loss function (QLF) would be smaller-is-better; the SNR of which is determined as expressed by equation (7):

$$\text{SN}_\text{S} = 10 \log \left(\frac{1}{\text{n}} \sum_{\text{i}=1}^{\text{n}} \text{y}_1^2 \right) \quad (7)$$

Where:
y_i = Core Losses for each experiment; and
n = Number of Experiments (in this case 9)

Plate 1: HIL Set-up for Running the Taguchi L9 Orthogonal Array Experimental Levels

FEM 3D Modeling and Validation

The Magnetostatic Solver in the ANSYS Maxwell, analyzed the static magnetic field under steady-state DC conditions to prevent exceeding core material saturation limits. An Eddy current solver evaluated AC losses at 50 Hz, reflecting the Nigerian grid's operational conditions. Boundary conditions simulated an open-circuit state, with a 2-meter distance from the core to minimize edge effects. Conditions were applied to ensure realistic magnetic field behavior, accurately reflecting the optimized flux density and Amorphous Steel properties. Maxwell's equations were numerically solved to simulate electromagnetic fields, flux distributions, and potential gradients within the core and windings, considering the nonlinear B-H characteristics of the Amorphous Steel. The core area (A_i) of the transformer is evaluated by the expression:

$$A_i = \frac{E_t}{4.44 f B_m} \tag{8}$$

The relationship between the diameter of the innermost part of the winding and the core cross-sectional area A_i is evaluated as:

$$A_i = kd^2 \tag{9}$$

Then, total losses (P_{Losses}) within the transformer are evaluated as:

$$P_{Losses} = P_C + P_i + Stray\ Load\ Losses \tag{10}$$

And since the efficiency (η) is maximum when; $\frac{d\eta_x}{dx} = 0$, then;

$$P_i = (x)^2 P_c \tag{11}$$

As reported by Hyun-Mo *et al.* (2012), the three Maxwell's equations used in the solver for electromagnetic field problems are:

$$\nabla \times H = \sigma(E) \tag{12}$$

$$\nabla \times E = -\frac{\partial B}{\partial t} \tag{13}$$

$$\nabla \times D = \rho \tag{14}$$

Where the following two equations result directly from the above equations:

$$\nabla \times \frac{1}{\sigma} \nabla \times H + \frac{\partial B}{\partial t} = 0 \tag{15}$$

$$\nabla \times B = 0 \quad (16)$$

The material properties involved in these equations are:
σ: Electric conductivity
ϵ: Dielectric permittivity
μ: Magnetic permeability
The final solution involved representing vector fields (such as $\vec{E}$ and $\vec{H}$) using first-order edge elements, and scalar fields (such as potentials) using second-order nodal unknowns. The field equations were coupled with circuit equations for both solid and stranded conductors, because in cases where voltage was applied, the resulting currents were not known apriori; and must be determined as part of the solution (Leela-Nivashini *et al.*, 2020).

Experimental Validation of the Optimized Transformer
To validate the optimized transformer, two indirect loading experiments were carried out; namely:

i. Open Circuit Test, and;
ii. Short Circuit Test

The tests (as shown in Figures 2 and 3) were carried out to determine the efficiency of the optimized transformer at full load as well as to be able to predict its efficiency at various loads. The experimental equipment for the experiments is the same as HIL set up for the Taguchi DOE shown in Plate 1.
Open Circuit (OC) Test: The open circuit test arrangement is as illustrated in Figure 2(a), while the equivalent parameters are illustrated in Figure 2(b) along with the associated phasor diagram. For this test, one of the windings (HV side) was left open, while the other winding (LV side) was supplied at rated voltage (in this case the secondary voltage) and frequency through an autotransformer. The voltage was adjusted using the autotransformer until the rated voltage was obtained. At the rated voltage (415V), the readings of the wattmeter (input power W_0) and ammeter (no-load current I_0) were recorded. Since the secondary was open circuited, the no-load current required to set up excitation in the primary winding is very small (usually 2. – 6% of the full-load current). The following parameters were measured during the OC test: W_0, I_0, V_1 and V_2. Considering Figure 8(a), the wattmeter reading W_0 is the input power to the primary winding, since the secondary is open circuited.

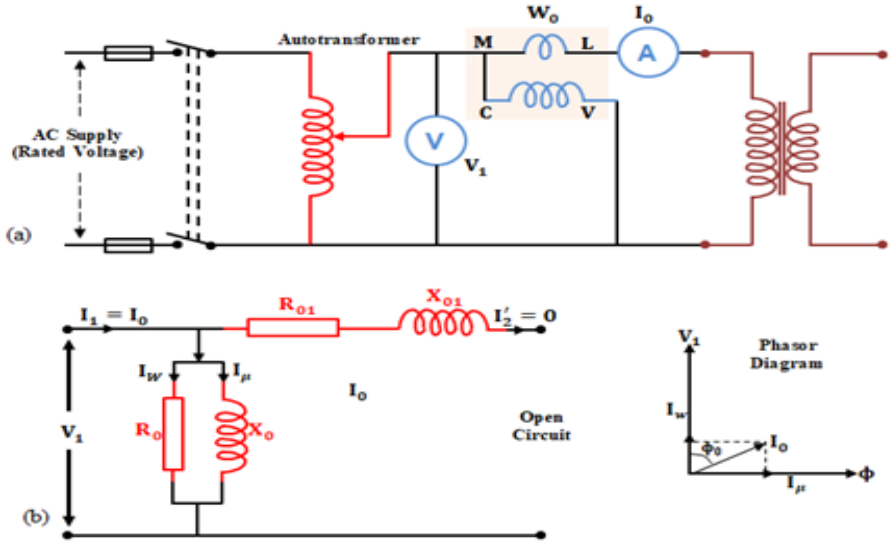

Figure 2: (a) Circuit arrangement for the Open Circuit (OC) Test Experimental Set-up, (b) Equivalent Parameters of the No-load Current (I_0) Branch

Considering Figure 2(b) (the equivalent circuit of the no-load current branch), current I_2' is the equivalent secondary current referred to the primary (no-load current branch) under no-load conditions. This current equals zero, as the secondary is open-circuited. This in effect means that $I_1 = I_0$. The no-load current I_0 consists of two components; namely the working component I_w and the magnetizing component I_μ, as shown in the phasor diagram (Figure 2[b]). Thus:

$$\text{Input power}(W_0) = V_1 I_0 \cos\phi_0 \quad (17);$$

So that $\cos\phi_0 = \frac{W_0}{V_1 I_0}$

The core loss component (I_w) of the current I_0 is given as $I_0 \cos\phi_0$, while the magnetizing component (I_μ) is given as $I_0 \sin\phi_0$.
Then:

$$\text{Core loss Resistance } R_0 = \frac{V_1}{I_w}\Omega \quad (18)$$

And:

$$\text{Magnetizing Reactance } X_0 = \frac{V_1}{I_\mu}\Omega \quad (19)$$

Thus:

$$W_0 = \text{Input Power} = \text{Output Power} + \text{Losses}$$
$$W_0 = \text{Output Power} + \text{Losses} = \text{Output Power} + \text{Core Losses} + \text{Copper Losses}$$
$$W_0 = 0 + \text{Core Losses} + 0 = \text{Core (Iron) Losses}$$

Now, $Copper\ Loss\ (W_{SC}) = I^2 R_{01}$ (20)

And the short circuit impedance is then determined as:

$$Z_{01} = \frac{V_{SC}}{I_{SC}} \quad (21)$$

$$\text{And the Leakage Reactance}(X_{01}) = \sqrt{Z_{01} - R_{01}} \quad (22)$$

Short Circuit (SC) Test: The short circuit test was carried out on the optimized transformer by applying 2% of the rated voltage at the primary winding (HV side), while the secondary winding (LV side) was short-circuited. This was done by adjusting the autotransformer until the full-load current I_{SC} was circulated in both windings (as measured by the ammeter). The circuit arrangement is as shown in Figure 3(a), while Figure 3(b) shows the equivalent circuit. Thus:

$$W_{SC} = \text{Input Power} = \text{Output Power} + \text{Losses}$$
$$W_{SC} = \text{Output Power} + \text{Losses} = \text{Output Power} + \text{Core Losses} + \text{Copper Losses}$$
$$W_{SC} = 0 + 0 + \text{Copper Losses} = \text{Copper}(I^2R)\text{Losses}$$

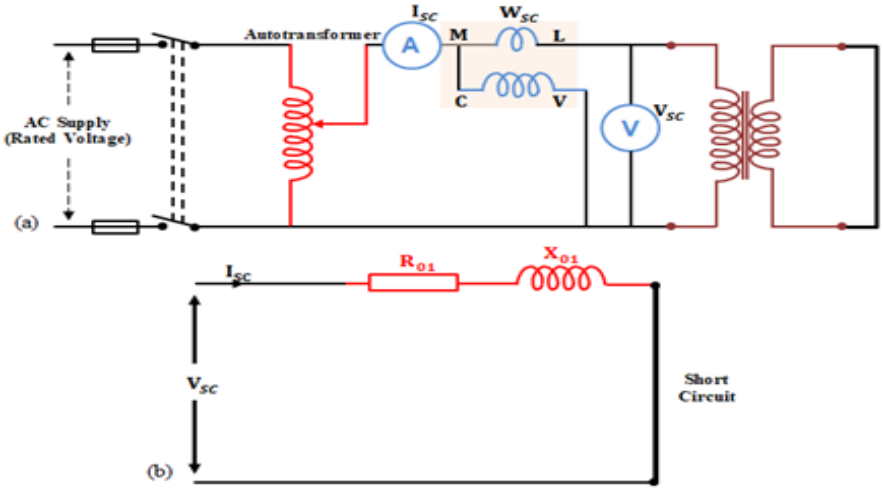

Figure 3: Circuit Arrangement for Short Circuit (SC) Test

Results

The Taguchi Experimental Results and Analysis

The experiments to determine the response variable (which is in fact, the core losses) were carried out using the experimental Hardware-In-the-Loop (HIL) set-up shown in Plate 1. Table 5 reflects the updated L9 Orthogonal Array with recorded core losses for each run.

Table 5: Updated L9 OA with recorded core losses for each run

Exp. Run	Core Area (m^2)	Core Material	Stepped Core Design	Flux Density (T)	(y_i) Core Losses (W/kg)
1	0.727	M5 Steel	Square Core	1.44	10.5
2	0.727	M6 Steel	Three-Stepped Core	1.526	12.8
3	0.727	Amorphous Steel	Six-Stepped Core	1.354	9.7
4	0.773	M5 Steel	Three-Stepped Core	1.526	11.2
5	0.773	M6 Steel	Six-Stepped Core	1.354	9.0
6	0.773	Amorphous Steel	Square Core	1.44	10.0
7	0.819	M5 Steel	Six-Stepped Core	1.354	12.0
8	0.819	M6 Steel	Square Core	1.44	11.5
9	0.819	Amorphous Steel	Three-Stepped Core	1.526	13.0

To initialize the signal-to-noise-ratio analysis, it is necessary to calculate the average of all the (y_i^2). Thus:

$$\text{Mean of Squared Values}\left(\frac{1}{n}\sum_{i=1}^{n} y_1^2\right) = \frac{y_1^2 + y_2^2 + y_3^2 + y_4^2 + y_5^2 + y_6^2 + y_7^2 + y_8^2 + y_9^2}{n}$$

$$= \frac{110.25 + 163.84 + 94.09 + 125.44 + 81.00 + 100.00 + 144.00 + 132.25 + 169.00}{9}$$

$$= 123.23$$

So that to calculate the overall SNR, we apply Equation (7):

$$SNR = -10\log_{10}(123.23) = -10 \times 2.091 \approx -20.91dB$$

Table 6 presents the updated L9 OA with the included (y_i^2) values, necessary for the signal-to-noise-ratio (SNR) analysis for each experimental run. Each entry in the response variable (y_i) column is squared to obtain the corresponding (y_i^2) value. The calculated SNRs are also updated in the Table; each against its corresponding experimental run.

Table 6: Updated table with included y_i^2 values and calculated SNRs

Exp. Run	Core Area (m^2)	Core Material	Stepped Core Design	Flux Density (T)	(y_i) Core Losses (W/kg)	(y_i^2) W^2/kg^2)	SNR (dB)
1	0.727	M5 Steel	Square Core	1.44	10.5	110.25	-20.91
2	0.727	M6 Steel	Three-Stepped Core	1.526	12.8	163.84	-22.12
3	0.727	Amorphous Steel	Six-Stepped Core	1.354	9.7	94.09	-19.76
4	0.773	M5 Steel	Three-Stepped Core	1.526	11.2	125.44	-20.98
5	0.773	M6 Steel	Six-Stepped Core	1.354	9.0	81.00	-19.08
6	0.773	Amorphous Steel	Square Core	1.44	10.0	100.00	-20.00
7	0.819	M5 Steel	Six-Stepped Core	1.354	12.0	144.00	-21.58
8	0.819	M6 Steel	Square Core	1.44	11.5	132.25	-21.30
9	0.819	Amorphous Steel	Three-Stepped Core	1.526	13.0	169.00	-22.28

Determination of the Taguchi Optimal Settings

The next step was the determination of the optimal parameter settings based on the SNRs. In the Taguchi method, the objective is to maximize the SNR for a "smaller-the-better" response, which is the case for minimizing core losses. The process proceeded as follows:

i. **Calculation of the mean SNR for Each Level**: For each factor (Core Area, Core Material, Stepped Core Design, and Flux Density), the mean S/N ratio at each level was calculated. This involved averaging the SNRs across the experiments where that particular level of the factor was used.

ii. **Identification of the Optimal Level for Each Factor**: For each factor; the level with the highest mean SNR was considered the optimal level, as it corresponded to the minimum value of the core losses.

iii. **Determination of the Optimal Parameter Settings**: Once the optimal levels for each factor were identified, the optimal parameter settings that should result in the best performance (minimum core losses) were determined.

Table 7 provides a clear representation of the calculated mean SNR for each parameter and its corresponding levels.

Table 7: The mean SNR calculations for each level

Parameter	Level	Runs	SNRs (dB)	Mean SNR (dB)
Core Area (m^2)	Level 1 (0.727)	Run 1, Run 2, Run 3	-20.91, -22.12, -19.76	-20.93
	Level 2 (0.773)	Run 4, Run 5, Run 6	-20.98, -19.08, -20.00	-20.02
	Level 3 (0.819)	Run 7, Run 8, Run 9	-21.58, -21.30, -22.28	-21.72
Core Material	M5 Steel	Run 1, Run 4, Run 7	-20.91, -20.98, -21.58	-21.16
	M6 Steel	Run 2, Run 5, Run 8	-22.12, -19.08, -21.30	-20.83
	Amorphous Steel	Run 3, Run 6, Run 9	-19.76, -20.00, -22.28	-20.68
Stepped Core Design	Square Core	Run 1, Run 6, Run 8	-20.91, -20.00, -21.30	-20.74
	Three-Stepped Core	Run 2, Run 4, Run 9	-22.12, -20.98, -22.28	-21.79
	Six-Stepped Core	Run 3, Run 5, Run 7	-19.76, -19.08, -21.58	-20.14
Flux Density	Nominal Value (1.44 T)	Run 1, Run 6, Run 8	-20.91, -20.00, -21.30	-20.74
	Lower Value (1.354 T)	Run 3, Run 5, Run 7	-19.76, -19.08, -21.58	-20.14
	Upper Value (1.526 T)	Run 2, Run 4, Run 9	-22.12, -20.98, -22.28	-21.79

Optimal Parameter Settings

The optimal settings based on the Taguchi robust DOE are:

i. Core Area: 0.773m^2
ii. Core Material: Amorphous Steel
iii. Stepped Core Design: Six-Stepped Core
iv. Flux Density: 1.354 T

These optimized settings along with other determined design parameters provide the most essential user-inputs in ANSYS Maxwell for the computer aided finite element method/analysis and physical/working design and validation of the optimized transformer.

Finite Element (Method) Analysis (FEA) for the Optimized Transformer Design

The optimized transformer underwent comprehensive FEA to assess its electromagnetic behavior, starting with Taguchi-determined optimal parameters: a core area of 0.773 m^2, Amorphous Steel material, a six-stepped core design, and a flux density of 1.354T. The transformer's geometry was modeled according to the six-stepped core, maintaining the core area to minimize losses and optimize flux distribution. Windings were placed within the core's window, with the Amorphous Steel specified for its reduced losses. Non-essential components were excluded, focusing on the core, windings, and insulation, treating the iron core as a single entity with simplified cylindrical windings.

Meshing Strategy

An adaptive meshing technique was used to refine the mesh around critical areas, such as the core corners and regions near the windings, to capture fine details of the electromagnetic fields. The model was meshed with

3,619,860 elements and 1,206,620 nodes, ensuring a maximum skewness of 0.6. A maximum element size of 0.1mm was used for the core and 0.025mm for the winding areas to ensure sufficient accuracy in regions of high flux concentration and rapid field changes.

Simulation

The simulations were executed with a total time of 38.6ms for the magnetic transient analysis to capture the initial inrush currents and their decay. For the steady-state analysis, the simulation was run until the results converged within a tolerance of 0.01%. Parameterization used equations (8, 9, 10, and 11) to evaluate characteristics like magnetic field strength, flux distribution, core losses, and thermal behavior. Maxwell's equations (equations 12 through 16) were solved within a finite region, with boundary and initial conditions set to simulate real-world operations. Magnetic symmetry planes ($H = 0$) simulated symmetry along the x-z and y-z planes, while open boundary conditions were set at 2000mm from the core. Environmental factors included a 10W/m²K convection boundary for cooling and insulation with a dielectric constant of $\varepsilon = 2.2$. The magnetic flux density was initialized at 0.169T, ensuring proper transient analysis. Windings were excited at 11kV (primary) and 0.415kV (secondary), generating the magnetic flux for steady-state conditions. Time-varying voltage and current excitations simulated real-world AC conditions, enabling analysis of core losses and transient events like ferroresonance, with a +100% voltage perturbation capturing overvoltage scenarios. M5 Steel was specified in the baseline model, as well as the specified parameters in Table 5, while Taguchi optimized key parameters including Amorphous Steel, core properties and flux density were specified in the optimized design. Four solvers—Electrostatic, Magnetostatic, Eddy Current, and Magnetic Transient—were applied to capture various electromagnetic phenomena.

Figure 4 illustrates the transformer model, highlighting both the core and windings in green. The figure clearly shows all three dimensions along the x, y, and z axes. The winding excitation is applied in the x-z plane, aligning with the magnetic flux path of the transformer to accurately simulate its electromagnetic behavior. The final 3D meshed model is shown in Figure 5. Figure 6(a) shows the energy density for both the baseline and optimized transformers during the initial excitation; while Figures 6(b) and 6(c) depict the respective energy densities of the transformers at maximum flux density. The computed field distributions and flux densities during initial excitation are shown in Figure 7(a); while Figures 7(b) and 7(c) depict field distributions at maximum flux density; for the baseline and optimized transformer, respectively. The B-H curves for both the baseline and optimized transformers are shown in Figures 8(a) and 8(b) respectively. The calculated mean core losses of the baseline and the optimized transformers are plotted as shown in Figures 9(a) and 9(b) respectively.

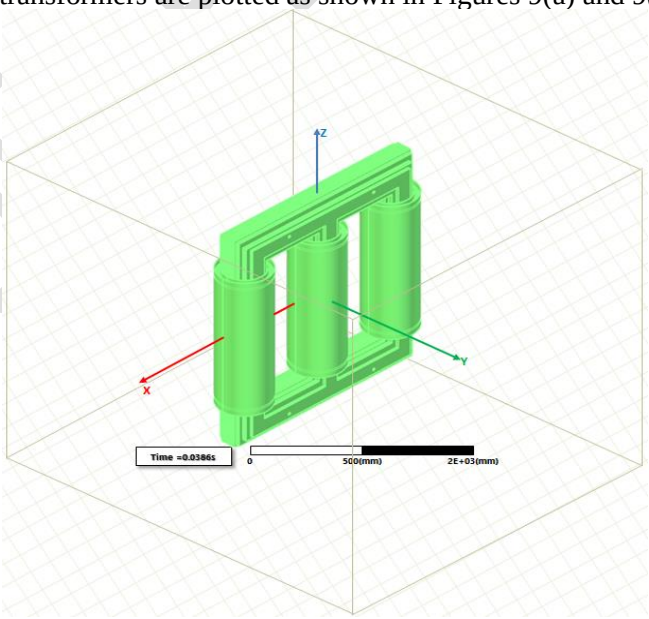

Figure 4: Designed 3D Model of the Transformer

Figure 5 shows the final 3D meshed model used for the FEA. The meshing was a critical step in the simulation, where the core and windings were discretized into elements to solve the electromagnetic field equations. The

model consists of 3,619,860 elements and 1,206,620 nodes, with an adaptive mesh refinement applied to ensure accuracy in regions of high flux concentration, such as the core corners and winding edges.

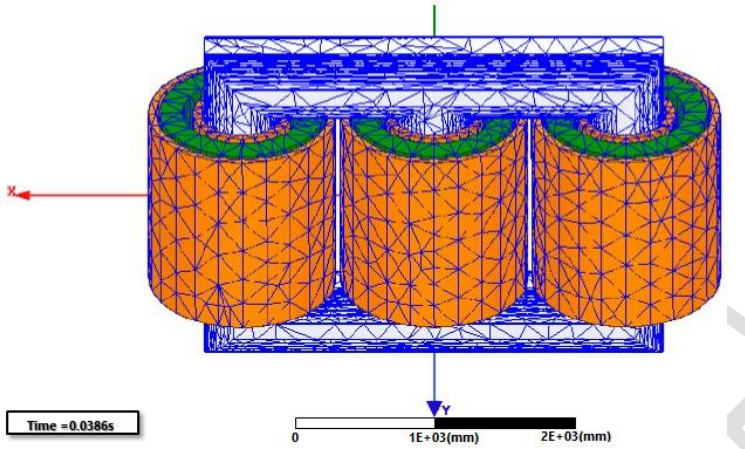

Figure 5: Final 3D Meshed Model of the Designed Transformer

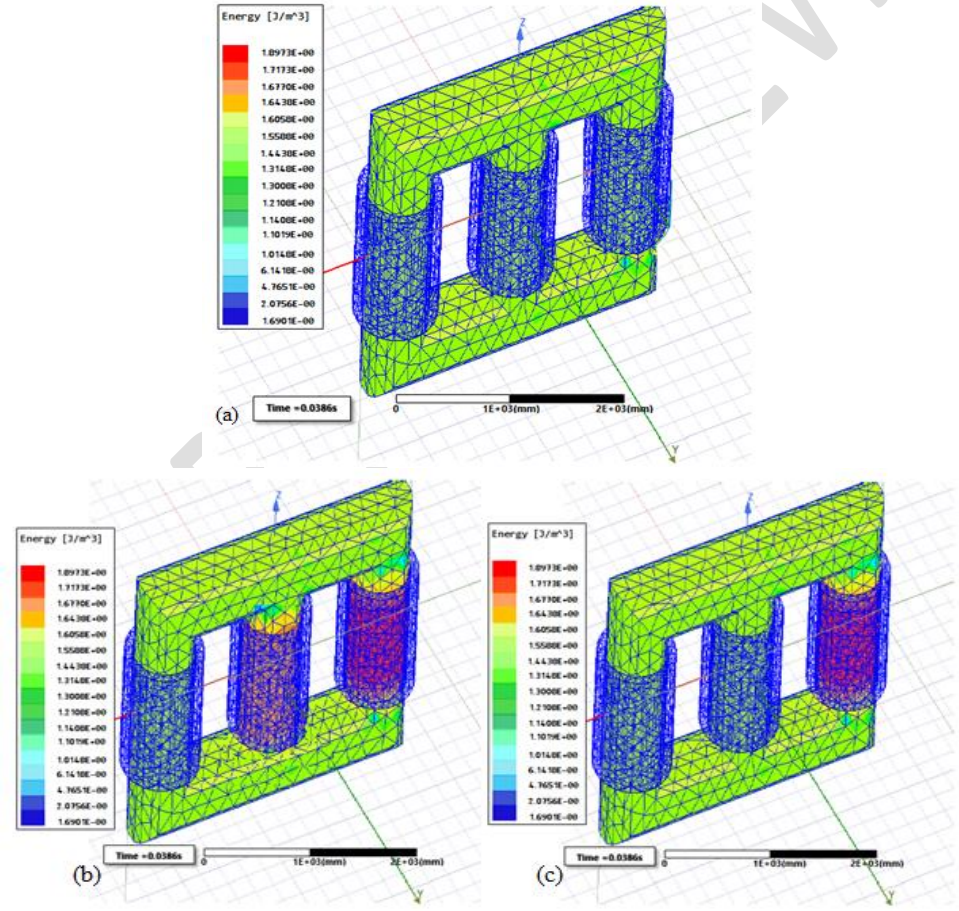

Figure 6: (a) Energy Density for Both Baseline and Optimized Transformers during Initial Excitation, (b) Energy Density of the Baseline Transformer at Maximum Flux Density, (c) Energy Density of the Optimized Transformer at Maximum Flux Density

Figure 6(a) illustrates the energy density distribution for both the baseline and optimized transformers during the initial excitation. At this stage, the flux is yet to fully stabilize, and both transformers exhibit uniform energy density distribution around the core. In Figures 6(b) and 6(c), the energy density distributions at maximum flux density for the baseline and optimized transformers are displayed. At this stage, the flux has fully stabilized,

and both transformers exhibit energy density concentrations of around $1.8973 J/m^3$ near the core-winding interface on the right limb. The baseline transformer however exhibits higher energy density; with additional concentration of roughly $1.6438 J/m^3$around the core-winding interface on the center limb. Higher localized energy densities, particularly in the core corners, could lead to increased localized core losses. The optimized transformer's lower energy density footprint is indicative of reduced core saturation and improved efficiency.

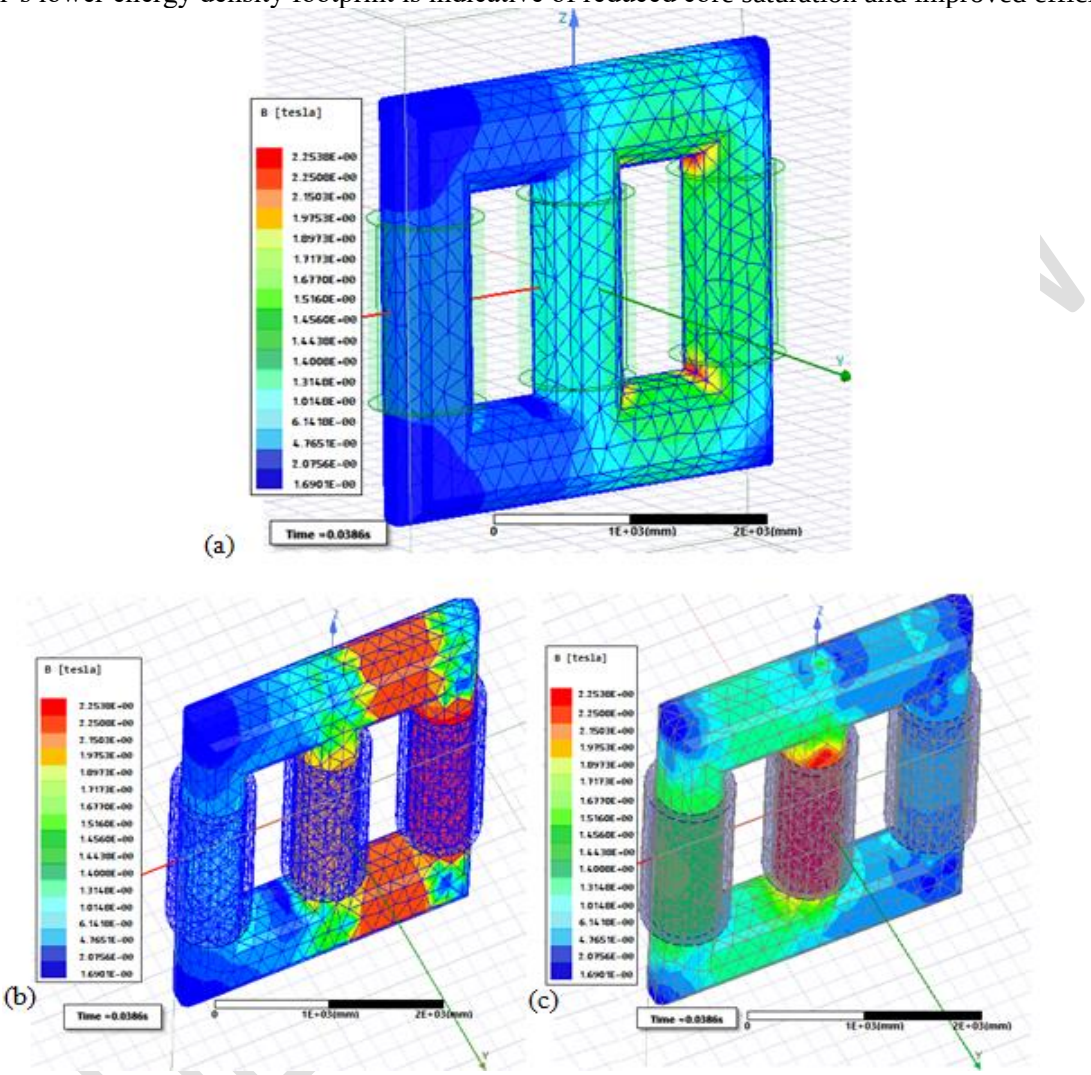

Figure 7: (a) Computed Field Distributions and Flux Densities during Initial Excitation, (b) Field Distributions for Baseline Transformer at maximum flux density, (c) Field Distributions for Optimized Transformer at maximum flux density

Figure 7(a) shows the magnetic field distribution during the initial excitation for both transformers, with less than 1.3148T flux density concentration in more than 80% of the cores although, the baseline transformer experiences slightly higher field concentrations, especially around the core joints and corners, which may contribute to higher inrush currents. The optimized transformer, on the other hand, demonstrates a more even field distribution, reducing stress on the core material during energization. Figures 7(b) and 7(c) depict the magnetic field distribution at maximum flux density for the baseline and optimized transformers, respectively. The optimized transformer shows a more balanced distribution, leading to reduced core saturation (around 19.2%) and more efficient magnetic performance. In contrast, the baseline transformer has higher field intensities (well above 1.7173T), particularly in the core limbs and yoke (with core saturations elevated to about 42%), which could result in elevated losses under full-load conditions.

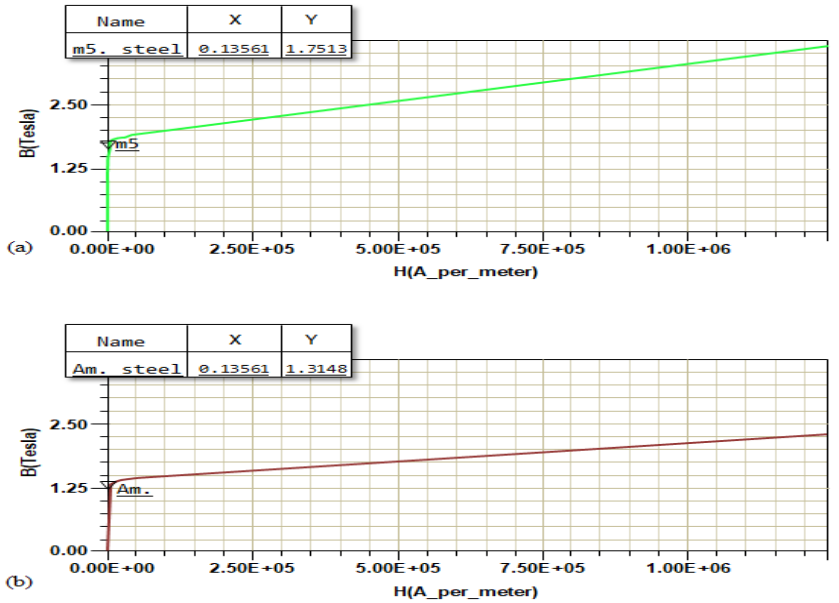

Figure 8: (a) B-H Curve for the Baseline Transformer, (b) B-H Curve for the Optimized Transformer

Figures 8(a) and 8(b) present the B-H curves for the baseline and optimized transformers, respectively. The baseline transformer reaches magnetic saturation at a lower magnetic field strength (≈ 2.50T at 5×10^5A/M) compared to the optimized transformer. The baseline transformer also exhibits a steeper B-H curve, indicating that it saturates more quickly as the magnetic field strength increases, which leads to higher core losses and reduced efficiency. In contrast, the optimized transformer B-H curve shows a more linear relationship over a wider range, exhibiting 1.75T at 5×10^5 A/M, and reflecting lower hysteresis losses as well as delayed saturation. This behavior indicates that the optimized transformer can handle higher magnetic field strengths without saturating, resulting in improved magnetic performance and overall efficiency.

Figures 9(a) and 9(b) plot the calculated average core losses for both the baseline and optimized transformers. The baseline transformer, due to the higher flux density, demonstrates higher core losses (average of 1.4317kW), particularly at higher loads. The core losses for the optimized transformer are reduced by approximately 27% (average of 0.8639kW) thereby minimizing hysteresis and eddy current losses.

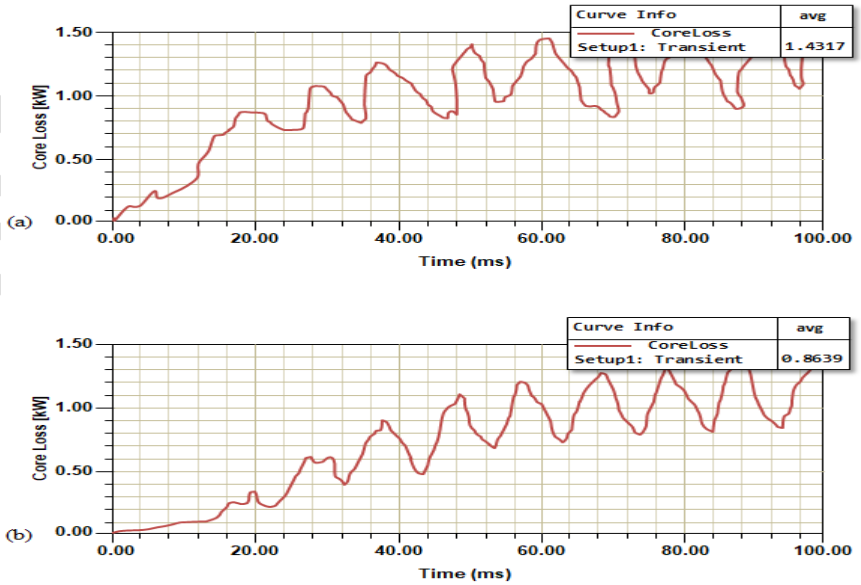

Figure 9: Calculated Average Core Losses for the Baseline Transformer, (b) Calculated Average Core Losses for the Optimized Transformer

Open Circuit (OC) Test Results
The recorded data from the open circuit tests were as follows: $V_1 = 415V$, $I_0 = 0.35A$, $W_0 = 65W$
Thus the Power Factor was determined as:

$$\cos\phi_0 = \frac{W_0}{V_1 I_0} = \frac{65}{415 \times 0.35} = 0.45$$

So that:
$I_w = I_0 \cos\phi_0 = 0.35 \times 0.45 = 0.1575A$

Now, $\cos^{-1}(0.45) = 63.3°$

$\therefore I_\mu = I_0 \sin\phi_0 = 0.35 \times \sin(63.3°)$

$I_\mu = 0.35 \times 0.89 = 0.3115A$

The core loss resistance and the magnetizing reactance were then determined respectively as:

$R_0 = \frac{415}{0.1575} = 2635\Omega$; $X_0 = \frac{415}{0.3115} = 1332\Omega$

Short Circuit (SC) Test Results
The readings on the wattmeter W_{SC}, ammeter I_{SC} and voltmeter V_{SC} were then recorded as:

$W_{SC} = 780W$, $I_{SC} = 41.2A$, $V_{SC} = 220V$

So that:

$$R_{01} = \frac{W_{SC}}{I_{SC}^2} = \frac{780}{(41.2)^2} \approx 0.4595\Omega$$

And the equivalent impedance can be determined from the relation:

$$Z_{01} = \frac{220}{41.2} \approx 5.34\Omega$$

$$(X_{01}) \approx \sqrt{(5.34)^2 - (0.4595)^2} \approx 5.299\Omega$$

The Comparison of Results for the Baseline and Optimized Transformers are presented in Table 8. The optimized transformer achieved an efficiency of approximately 97.15% at full load. With core losses of 85W and copper losses of 800W, the output power was measured at 29.2kW from an input of 30 kVA. These results demonstrate the success of the optimized design in minimizing energy losses, making it highly efficient and suitable for reliable, low-loss power delivery in real-world applications.

Table 8: Comparison of results for the baseline and optimized transformers

Parameter	Baseline Transformer	Optimized Transformer
Rated Power	30 kVA	30 kVA
Primary Voltage	11 kV	11 kV
Secondary Voltage	0.415 kV	0.415 kV
Frequency	50 Hz	50 Hz
Short Circuit Impedance	6%	5.34%
Flux Distribution	Higher losses due to less optimized design	Optimized for better distribution

Optimal Energy Density	Moderate (due to conventional design)	Higher efficiency (due to improved design)
Total Harmonic Distortion (THD)	16.78%	4.12%
Lowest Harmonic Distortion (THD)	13.57%	3.28%
Harmonic Susceptibility	Higher, needs mitigation	Improved resilience due to optimized design
No-load Loss	340 W	85 W
Load Loss (75°C)	1070 W	800 W
Load Loss (120°C)	1230 W	820 W
No-load Current (%)	2.4%	2.32%
Core Loss Resistance (Ω)	2150 Ω	2550 Ω
Magnetizing Reactance (Ω)	1100 Ω	1285 Ω
Copper Loss Resistance (Ω)	0.2047Ω	0.153Ω
Copper Loss Reactance (Ω)	3.04Ω	3.04Ω
Efficiency at Full Load (%)	95.5%	97.15%
Efficiency at 90% Load	95.7%	98.37%
Efficiency at 80% Load	96.5%	98.5%
Efficiency at 75% Load	96.7%	98.6%
Efficiency at 65% Load	97.0%	98.8%
Efficiency at 50% Load	97.4%	99.1%

Discussion

The optimization process using the Taguchi method and SNR analysis identified the ideal transformer design parameters: core area, material, core design, and flux density. A core area of 0.773 m² balanced core losses and magnetic efficiency, with Amorphous Steel emerging as the superior material, with SNR of -20.68 dB indicated lower energy losses than M5 and M6 Steel. This finding aligns closely with Geetha et al. (2024) but contrasts with Pramono et al. (2023), who reported higher SNRs due to different methods. The Six-Stepped Core design optimized flux distribution, and a flux density of 1.354T minimized energy losses by 27%, supporting findings by Sarac (2017), who reported increased losses in saturated cores.

FEA Analysis showed that the optimized transformer exhibited 19.2% core saturation, significantly lower than the baseline's 42%, with reduced energy density near the core-winding interface, affirming findings by Hacan et al. (2022) on efficiency impacts from core saturation. The B-H curve analysis indicated that the optimized transformer had a delayed saturation point (1.75T at 5×10^5 A/M), which reduced hysteresis losses compared to the baseline's (≈ 2.50T at 5×10^5A/M).

Open Circuit (OC) and Short Circuit (SC) tests showed efficiency gains: the optimized transformer's core losses reduced to 85W and copper losses to 800W, achieving 97.15% full-load efficiency, in line with IEC 60076-8 standards. These results align with Xinsheng et al. (2020), who documented reduced losses with enhanced core materials and design; as well as Hacan et al. (2022), who noted lower efficiency with differential evolution algorithm in ANSYS Maxwell.

This study addressed gaps in transformer design for low-voltage distribution systems, aligning with related works that stress balancing efficiency and harmonic resilience. Integrating Taguchi DOE and FEA in this study, provides insights into optimizing transformer performance, offering a basis for a wider range of applications.

Conclusion

This study has successfully optimized a 30 kVA transformer for enhanced efficiency and reduced harmonic susceptibility in low-voltage distribution systems. Utilizing a combination of Taguchi DOE, SNR analysis, and FEA, key design parameters—core area, core material, stepped core design, and flux density—were systematically optimized. The resulting transformer demonstrated a 27% reduction in core losses and achieved a full-load efficiency of 97.15%, as confirmed through OC and SC testing. These improvements align with IEC 60076-8 standards, marking a significant advance over baseline models and making the transformer highly suitable for reliable power delivery in real-world applications. The optimized transformer presents a robust design that balances performance and efficiency while minimizing energy losses in practical applications. This

study provides a foundation for future transformer designs in low-voltage networks, particularly in environments with harmonic challenges. The integration of Taguchi DOE and FEA into transformer optimization contributes valuable insights for researchers and practitioners aiming to improve energy efficiency and resilience in modern distribution systems.

Despite these promising results, certain limitations warrant attention. The study focused on a single transformer rating (30 kVA) and specific operating conditions, which may limit generalizability to other power ratings or network configurations. Additionally, the optimized design was validated primarily through laboratory testing; future work could expand testing to field conditions to better understand real-world performance under variable loads and environmental factors.

Future research could explore scaling the optimized parameters for transformers of varying capacities to evaluate performance across a broader range of distribution requirements. Additionally, further studies could integrate more advanced materials, such as nanocrystalline cores, which might offer improved performance but require cost-benefit analysis. Investigating resilience under extreme harmonic and ferroresonant conditions could provide insights into broader grid applications, potentially leading to enhanced designs for high-stress environments.

References

Abdulhamid, A. A. (2020). An optimized campus hybrid microgrid model based on technical and economic feasibility analysis. LAJAST: *Journal of Engineering, Science and Technology*, *4*(3), 1-17. https://www.asuplafia.org.ng/journal.

Arkadan, A. A., & Gutierrez-McCoy, M. A. (2023). Power transformer characterization and design optimization environment. IEEE Transactions on Magnetics, 59(5), 1-5. https://doi.org/10.1109/TMAG.2023.3237750.

Baldwin, B., Sabade, S. & Joshi, S. (2013). *A study of ferroresonance & mitigation techniques*. Michigan Technological University Course Lecture Material, 1-41. Retrieved from: http://www.ece.mtu.edu/faculty/bamork/EE5223/EE5223TermProj.pdf.

Barua, A., Deb, P. K., Maheshwari, R. & Tekade, R. K. (2018). Statistical techniques in pharmaceutical product development. In R. K. Tekade (Ed.), *Advances in Pharmaceutical Product Development and Research: Dosage Form Design Parameters* (pp. 339-362). Academic Press.

Box, G. E. P., Hunter, W. G. & Hunter, J. S. (2005). *Statistics for engineers: An introduction to design, data analysis, and model building*. New York: John Wiley & Sons.

Di-Noia, L. P., Lauria, D., Mottola, F. & Rizzo, R. (2017). Design optimization of distribution transformers by minimizing the total owning cost. *International Transactions on Electrical Energy Systems, 27*(11), 1-16. https://doi.org/10.1002/etep.2397.

Geetha, A., Balamurugan, K. S., Geetha, P., Jemimah Carmicharl, M. & Usha, S. (2024). Optimization of core loss for power transformer using Taguchi method. *EAI Endorsed Transactions on Energy Web, 11*(1), 1-10. doi: 10.4108/ew.5051.

Hamzaçebi, C. (2020). Taguchi method as a robust design tool. In P. Li, P. A. R. Pereira & H. Navas (Eds.), *Quality control - Intelligent manufacturing, robust design and charts* (pp. 2-22). Open Access Peer-Reviewed Chapter. DOI: 10.5772/intechopen.94908.

Hacan, A. F., Kabas, B. & Oguten, S. (2022). Design optimization of a three-phase transformer using finite element analysis. *Electrical Engineering and Systems Science: Systems and Control*. arXiv:2201.11769 [eess.SY]. https://doi.org/10.48550/arXiv.2201.11769.

Huang, S. J. & Hsieh, C. H. (2013). Relation analysis for ferroresonance of bus potential transformer and circuit breaker grading capacitance. *International Journal of Electrical Power & Energy Systems, 51*(10), 61-70. https://doi.org/10.1016/j.ijepes.2013.03.005.

Hyun-Mo, A., Yeon-Ho, O., Joong-Kyoung, K., Jae-Sung, S. & Sung-Chin, H. (2012). Experimental verification and finite element analysis of short-circuit electromagnetic force for dry-type transformer. *IEEE Transactions on Magnetics, 48*(1), 819-822. DOI: 10.1109/TMAG.2011.2174212.

Karna, S. K. & Sahai, R. (2012). An overview on Taguchi method. *International Journal of Engineering and Mathematical Sciences, 1*(1), 11-18.

Koledowo, S. O., Ashigwuike, E. C. & Bawa, A. (2020). A study of ferroresonance in underground distribution network for 15MVA, 33/11 kV injection substation. *Nigerian Journal of Technology (NIJOTECH), 39*(1), 219-227. http://dx.doi.org/10.4314/njt.v39i1.25.

Kraszewski, W., Syrek, P. & Mitoraj, M. (2022). Methods of ferroresonance mitigation in voltage transformers in a 30 kV power supply network. *Energies, 15*(24), 1-17. https://doi.org/10.3390/en15249516.

Leela Nivashini, M., Madhumitha, K., Sindhu, S. & Maheswari, R. V. (2020). Design of high voltage transformer using finite element method. *International Journal of Scientific & Technology Research, 9*(3), 5351. Retrieved from http://www.ijstr.org.

Ntemi, M., Paraschos, S., Karakostas, A., Gialampoukidis, I., Vrochidis, S. & Kompatsiaris, I. (2022). Infrastructure monitoring and quality diagnosis in CNC machining: A review. *CIRP Journal of Manufacturing Science and Technology, 38*(1), 631-649. https://doi.org/10.1016/j.cirpj.2022.06.001.

Olivares-Galvan, J. C., Ascencion-Mestiza, H., Maximov, S., Mezura-Montes, E. & Escarela-Perez, R. (2023). Design of a three-phase shell-type distribution transformer using evolutionary algorithms. *Energies, 16*(4016), 1-16. doi:10.3390/en16104016.

Oliveira, J. C. (2022). Sustainable processing: Continuous process improvement and optimization. In P. L. H. McSweeney & J. P. McNamara (Eds.), *Encyclopedia of dairy sciences* (3rd ed., pp. 812-820). Academic Press.

Outzguinrimt, H., Chraygane, M., Lahame, M., Oumghar, R., Bouzit, A. & Ferfra, M. (2020). Optimal design of a three-phase magnetic flux leakage transformer for industrial microwave generators. *Bulletin of Electrical Engineering and Informatics, 9*(1), 57-66. doi:10.11591/eei.v9i1.1679.

Pramono, W. B., Wijaya, F. D., Hadi, S. P., Wahyudi, M. S. & Indarto, A. (2023). Designing power transformer using particle swarm optimization with respect to transformer noise, weight, and losses. *Designs, 7*(31), 1-22. doi:10.3390/designs7010031.

Rasmann, R., Golev, V., Schumann, U., & Schnack, J. (2023). Automated design and optimization of planar transformers for high-frequency applications. *2023 IEEE Design Methodologies Conference (DMC)*, 1-6. https://doi.org/10.1109/DMC58182.2023.10412480.

Sarac, V. (2017). FEM 2D and 3D design of transformer for core losses computation. In *Scientific Proceedings XIV International Congress "Machines. Technologies. Materials." 2017 - Summer Session. Faculty of Electrical Engineering, University* "Goce Delcev", R. Macedonia.

SIMTEQ Engineering. (2024). Understanding computer aided engineering (CAE): Applications, advantages, and how to make the most of it in your company. Blogs. Retrieved from https://simteq.co.za/blog/understanding-computer-aided-engineering-cae-its-applications-advantages-and-how-to-make-the-most-of-it-in-your-company/.

Tsili, M. A., Amoiralis, E. I., Kladas, A. G. & Souflaris, A. T. (2012). Optimal design of multi-winding transformer using combined FEM, Taguchi, and stochastic-deterministic approach. *IET Electric Power Applications, 6*(7), 437-454. doi: 10.1049/iet-epa.2011.0310.

Vuchkov, I. N. & Boyadjieva, L. N. (2001). *Quality improvement with design of experiments: A response surface approach*. Dordrecht: Kluwer Academic Publishers.

Worku, M. Y. (2022). Recent advances in energy storage systems for renewable source grid integration: A comprehensive review. *Sustainability, 14*(10), 1-18. https://doi.org/10.3390/su14105985.

Xinsheng, Y., Yunpeng, Z., Guizhi, X., Changgeng, Z. & Weinong, F. (2020). Multi-objective optimization design of transformer based on T-ψ finite element method. *Transactions of China Electrotechnical Society, 36*(1), 75-83. https://doi.org/10.19595/j.cnki.1000-6753.tces.L90544.